PHYSICAL REVIEW B **96**, 144109 (2017)

Local strain heterogeneity and elastic relaxation dynamics associated with relaxor behavior in the single-crystal perovskite $Pb(In_{1/2}Nb_{1/2})O_3$-$PbZrO_3$-$Pb(Mg_{1/3}Nb_{2/3})O_3$-$PbTiO_3$

Wenhui He,[1,2] Michael A. Carpenter,[2,*] Giulio I. Lampronti,[2] Qiang Li,[1] and Qingfeng Yan[1,†]
[1]*Department of Chemistry, Tsinghua University, Beijing 100084, China*
[2]*Department of Earth Sciences, University of Cambridge, Cambridge CB2 3EQ, United Kingdom*

(Received 14 August 2017; revised manuscript received 21 September 2017; published 18 October 2017)

Recently, $Pb(In_{1/2}Nb_{1/2})O_3$-$PbZrO_3$-$Pb(Mg_{1/3}Nb_{2/3})O_3$-$PbTiO_3$ (PIN-PZ-PMN-PT) relaxor single crystals were demonstrated to possess improved temperature-insensitive properties, which would be desirable for high-power device applications. The relaxor character associated with the development of local random fields (RFs) and a high rhombohedral-tetragonal (R-T) ferroelectric transition temperature ($T_{\mathrm{R-T}} > 120\,^{\circ}\mathrm{C}$) would be critical for the excellent properties. A significant effect of the chemical substitution of In^{3+} and Zr^{4+} in PMN-PT to give PIN-PZ-PMN-PT is the development of local strain heterogeneity, which acts to suppress the development of macroscopic shear strains without suppressing the development of local ferroelectric moments and contribute substantially to the RFs in PIN-PZ-PMN-PT. Measurements of elastic and anelastic properties by resonant ultrasound spectroscopy show that PIN-PZ-PMN-PT crystal has a quite different form of elastic anomaly due to Vogel-Fulcher freezing, rather than the a discrete cubic-T transition seen in a single crystal of PMN-28PT. It also has high acoustic loss of the relaxor phase down to $T_{\mathrm{R-T}}$. Analysis of piezoresponse force microscopy phase images at different temperatures provides a quantitative insight into the extent to which the RFs influence the microdomain structure and the short-range order correlation length $\langle \xi \rangle$.

DOI: 10.1103/PhysRevB.96.144109

I. INTRODUCTION

There has been close interest in how local structure can have a significant impact on the macroscopic physical properties of ferroelectric relaxor materials. In 2008, based on neutron inelastic-scattering results, Xu *et al.* [1] reported that a strong interaction between polar nanoregions (PNRs) and the propagation of acoustic phonons perhaps contributes to the ultrahigh piezoelectric response of $Pb(Zn_{1/3}Nb_{2/3})O_3$-4.5%$PbTiO_3$ single crystals. Li *et al.* [2,3] reported that large piezoelectric effects are due to 50–80% contribution from PNRs at room temperature, where the PNRs behave as "seeds" to facilitate macroscopic polarization rotation and enhance electric-field-induced strain. $Pb(In_{1/2}Nb_{1/2})O_3$-$PbZrO_3$-$Pb(Mg_{1/3}Nb_{2/3})O_3$-$PbTiO_3$ represents one example of remarkable relaxor materials with high ferroelectric (FE) phase-transition temperature ($T_{\mathrm{FE-FE}} > 120\,^{\circ}\mathrm{C}$) and excellent piezo-/dielectric properties ($d^{*}_{33[001]} > 1000\,\mathrm{pm/V}$, $\varepsilon_{33[001]} = 4000$) [4,5]. The relaxor character is related to enhanced B-site disorder but, in the case of $0.5Ba(Zr_{0.2}Ti_{0.8})O_3$-$0.5(Ba_{0.7}Ca_{0.3})TiO_3$, it has been shown that local strain heterogeneity influenced by the substitution of cations with different ionic radii in the ABO_3 perovskite structure acts as a major factor in the development of adaptive microstructures and the enhanced piezoelectric properties [6]. With respect to applications of piezoelectric and ferroelectric materials with dramatically improved temperature-insensitive properties, a key focus is therefore on the microstructures and strain-coupling effects as a function of temperature in $Pb(In_{1/2}Nb_{1/2})O_3$-$PbZrO_3$-$Pb(Mg_{1/3}Nb_{2/3})O_3$-$PbTiO_3$ relaxor single crystal with decreasing length scale for the PNRs.

Resonant ultrasound spectroscopy (RUS) has proved to provide a particularly sensitive window on relaxor behavior and microstructure dynamics through observations of elastic and anelastic anomalies which accompany strain-relaxation phenomena in mm-sized single crystal and ceramic samples across wide temperature intervals [7–9]. The states and properties of interest, relating to polarization and permittivity, are first- and second-rank tensor quantities, respectively, while strain and elastic moduli are second- and fourth-rank tensor quantities [10]. It follows that elastic responses, in particular, can convey additional information on the form, magnitude, and symmetry of the coupling processes which are influenced by the relaxor behavior. Importantly, the variations of polarized microstructures such as PNRs and tweed/twin structures can also be investigated through their anelastic behavior in terms of the inverse mechanical quality factor Q^{-1}, even when the magnitudes of strains are on the order of or less than 1% [11,12]. While RUS provides a means of investigating microstructure dynamics indirectly, via the elastic and anelastic responses, piezoresponse force microscopy (PFM) allows direct observations of domain structures at the micro-/nanoscale when the polarity is spatially fixed [13–15]. Based on PFM images, combined with autocorrelation analysis [16–18], the temperature-dependent relaxor behavior can also be viewed.

The primary objective of the present study was to investigate the elastic and anelastic relaxation behavior of single-crystal $28Pb(In_{1/2}Nb_{1/2})O_3$-$8PbZrO_3$-$36Pb(Mg_{1/3}Nb_{2/3})O_3$-$28PbTiO_3$ (henceforth "PIN-PZ-PMN-PT" in this work) with poling along the [001] cubic direction, $[001]_{\mathrm{C}}$, between ~10 and 700 K. Additional insights come from a comparison with similar data collected from a $[001]_{\mathrm{C}}$ PMN-28PT crystal with the same PT content because of the dissimilar length scale of PNRs that occur within them. The expected sequence of transitions with heating expected in both crystals

---

[*] mc43@cam.ac.uk
[†] yanqf@mail.tsinghua.edu.cn

is rhombohedral (R, $R3m$)-tetragonal (T, $P4mm$)-cubic (C, Pm-$3m$) [4,19]. The temperature-induced domain evolution has been investigated directly using PFM for unpoled PIN-PZ-PMN-PT single crystals and the temperature dependence of a short-range correlation length $\langle \xi \rangle$ has been extracted from PFM phase images using the autocorrelation function.

II. EXPERIMENTAL DETAILS

The 28PIN-8PZ-36PMN-28PT single crystal was grown by a slow-cooling method [4], and then cut into the shape of a rectangular parellelepiped with dimensions $1.52 \times 2.73 \times 0.38\,\mathrm{mm}^3$ (named sample 1, see Supplemental Material [20]). The largest faces were aligned parallel to (001) of the parent cubic structure, while the smaller faces were in arbitrary crystallographic orientations perpendicular to this. This was divided into two pieces via wire-cut technology. Both pieces were annealed at 500 °C for 24h. X-ray photoelectron spectroscopy (XPS) (PHI Quantera SXM$^{\mathrm{TM}}$) was performed on the (001) face of one of the pieces (named sample 2, $1.33 \times 1.47 \times 0.38\,\mathrm{mm}^3$, mass 0.0056 g, see Supplemental Material [20]) to characterize In, Zr contents, and oxygen stoichiometry. X-ray diffraction (XRD) patterns were then collected from (001) face in a D8 ADVANCE, Bruker diffractometer, with CuKα radiation in the range 15–50°.

Gold electrodes were sputtered on the (001) faces of sample 2, as used for dielectric and RUS measurements. A 1-kV/mm electric field was applied to pole the sample for 3 min at room temperature, parallel to [001] of the cubic structure, $[001]_{\mathrm{C}}$. Dielectric properties as a function of temperature were determined using an impedance analyzer (Agilent 4294A) at frequencies of 0.1–100 kHz. A polarization versus electric field (P-E) loop was measured at 493 K using an aixACCT TF Analyzer 2000E.

A PMN-28PT crystal was prepared and treated in the same way. The sample used for dielectric and RUS measurements had dimensions $4.14 \times 4.38 \times 0.79\,\mathrm{mm}^3$ and mass 0.0943 g. At the end of all experiments the crystals used for RUS were ground up and powder x-ray diffraction patterns were collected in the range 20–90°. Lattice parameters were provided by refinements using the software TOPAS4.1 [21].

The underlying principles of resonant ultrasound spectroscopy have been described extensively elsewhere [7,22,23]. For low-temperature RUS measurements [24], the PIN-PZ-PMN-PT single crystal was held with the (001) faces between a pair of piezoelectric transducers in an atmosphere of a few millibars of helium gas. Spectra containing 50 000 data points in the frequency range 0.1–1.2 MHz were collected between 10 and 295 K in ∼5-K steps, with a period of 20 min for thermal equilibration at each set point. In the high-temperature instrument [7], the crystal was held in air with a pair of corners resting lightly between the tips of two alumina buffer rods. Individual spectra again contained 50 000 points through a frequency range of 0.1–1.2 MHz in the temperature interval 295–700 K. The high-temperature spectra were collected in a series of stages, such as from 295–410 K in ∼5-K steps, from 410–500 K in ∼1-K steps, and from 500–700 K in ∼10-K steps, followed by cooling in the same sequence, with a thermal equilibration time of 20 min at each temperature. The same procedures were followed for the PMN-28PT crystal through the temperature intervals 10–295 K and 295–650 K. A small correction, based on calibration against the transition temperature of quartz (846 K), was applied to measured temperatures from the high-temperature instrument to allow for the fact that the measuring thermocouple is a few mm away from the sample.

Detailed analysis of all the RUS spectra was performed using the software package IGOR PRO (WaveMetrics). An asymmetric Lorentzian function was fit to individual peaks in order to determine their peak frequency f and the full width at half maximum height Δf. The elastic constants determining each resonance mode scale with f^2, but for a poled crystal the values are also dependent on relatively small contributions from the piezoelectric moduli. The inverse mechanical quality factor Q^{-1} can be expressed as $\Delta f/f$ to give a measure of acoustic loss. It is sensitive to transformation-related microstructures and provides further information about the dynamics of relaxor properties. Since the as-prepared samples did not have all faces parallel to $\{001\}$, the absolute values of elastic constants were not determined. However, the overall evolution of elastic and anelastic properties could be followed as a function of temperature with the additional understanding that the predominant motion involved in acoustic resonances of a small sample involves shearing. For a cubic crystal the square of the resonance frequencies f^2 depends mainly on $1/2(C_{11}-C_{12})$ and C_{44}.

The remaining piece of sample 1 of PIN-PZ-PMN-PT was ground down to a thickness of ∼70 μm and one of the (001) faces was polished to an optical finish. PFM images from the polished (001) surface were obtained *in situ* at a range of temperatures using a commercial atomic force microscope (Cypher, Asylum Research) with conducting EFM probes coated by Pt/Ir (force constant 2.8 N/m, resonance frequency 75 kHz) (NanoWorld). An ac excitation signal of 0.8 V was added at intervals of increasing temperature to measure the microdomains.

III. RESULTS AND DISCUSSION

A. XRD and XPS

In order to confirm the sample orientation and quality, an XRD pattern and XPS spectra were collected from the as-prepared $[001]_{\mathrm{C}}$ PIN-PZ-PMN-PT crystal. As shown in Fig. 1, two sharp diffraction peaks assigned to (001) and (002) planes are consistent with single-crystal perovskite structure in the expected crystallographic orientation. Comparison of x-ray powder-diffraction patterns from PIN-PZ-PMN-PT and PMN-28PT in Fig. S2 (see Supplemental Material [20]) shows peaks of the former shifted to lower angles, due to the incorporation of In^{3+} and Zr^{4+} with larger ionic radii than the ions which they replaced ($R_{\mathrm{In}^{3+}} = 0.81$ Å, $R_{\mathrm{Zr}^{4+}} = 0.79$ Å, $R_{\mathrm{Mg}^{2+}} = 0.65$ Å, $R_{\mathrm{Nb}^{5+}} = 0.70$ Å). More complete structure details are provided in Fig. S2 (see Supplemental Material [20]).

Segments of high-resolution XPS spectra for the PIN-PZ-PMN-PT single crystal are shown in the insets (a) and (b) of Fig. 1. They give banding energies of 444.0 eV for In $3d_{5/2}$ and 181.4 eV for Zr $3d_{5/2}$, which is in agreement with data

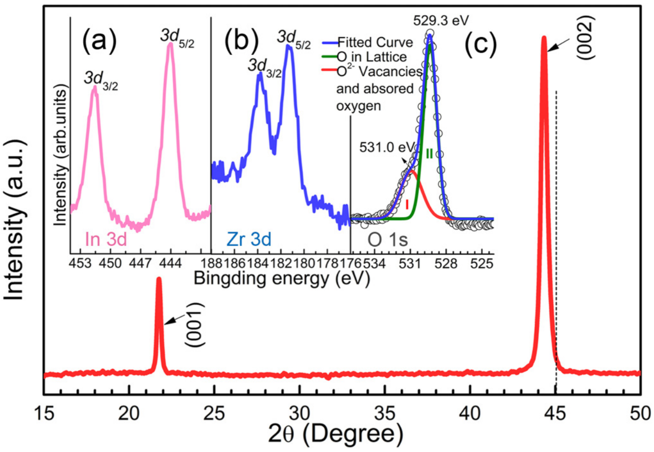

FIG. 1. Segment of the XRD pattern obtained from the as-prepared $[001]_C$ PIN-PZ-PMN-PT single crystal. The insets (a), (b), and (c) show high-resolution XPS spectra of the In $3d$, Zr $3d$, and O $1s$ signals, respectively.

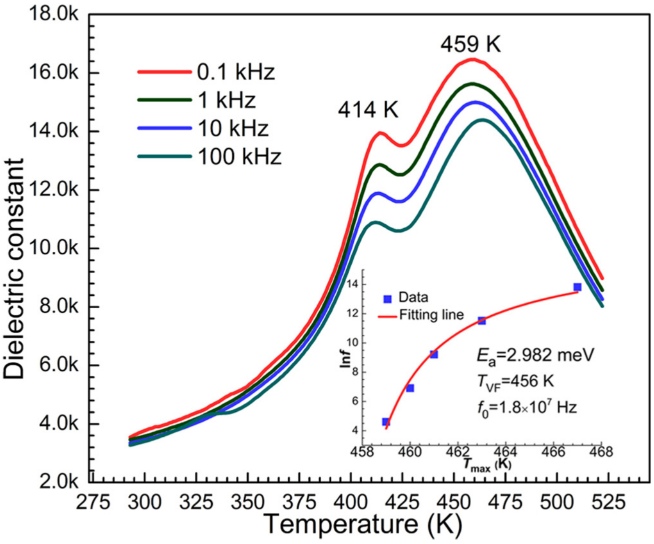

FIG. 2. Temperature-dependent dielectric permittivity for poled $[001]_C$ PIN-PZ-PMN-PT single crystal. The inset shows the frequency of maximum permittivity as a function of T_{max} and the curve is a fit of the Vogel-Fulcher equation.

reported elsewhere [25,26]. Inset (c) shows the O $1s$ signal and corresponding curve fitting using a Gaussian function to resolve two components. The peak of binding energy (BE) at 529.3 eV corresponds to oxygen in the PIN-PZ-PMN-PT lattice, including Pb–O, In–O, Zr–O, Ti–O, Mg–O, and Nb–O bonds. The BE of the component with lower intensity was close to 531.0 eV, and has been attributed to the presence of oxygen vacancies in crystals or chemically adsorbed oxygen on the crystal surface [27,28]. The ratio of areas under the peaks I and II is often used to estimate oxygen vacancy, and the area ratio A_I/A_{II} obtained here was 0.44, indicating a low oxygen vacancy concentration.

B. Dielectric properties

Figure 2 shows dielectric permittivity versus temperature for the poled $[001]_C$ PIN-PZ-PMN-PT crystal at multiple frequencies, collected in a heating sequence. The overt frequency dispersion near 459 K reveals relaxor character for the crystal. As reported in He *et al.* [5], the length scale of PNRs decreases due to the incorporation of In^{3+} and Zr^{4+}, in comparison with PMN-28PT single crystals with the same PT content. There is then a distinct FE phase transition at $T = 414$ K, which is much higher than in other relaxor systems [29].

Of particular significance is that the relationship between the temperature (T_{max}) of maximum permittivity and the frequency can be described in terms of Vogel-Fulcher (VF) dynamics according to [12,30,31]

$$f = f_0 \exp\left[-\frac{E_a}{k(T_{max} - T_{VF})}\right], \tag{1}$$

where E_a is the activation energy for relaxation, T_{VF} is the freezing temperature, f_0 is the attempt frequency, and k is the Boltzmann constant. The freezing process is generally understood to give rise to PNRs in a disordered matrix, while their boundaries may still be mobile. The inset of Fig. 2 shows a plot of $\ln(f)$ vs T_{max}, where blue rectangles are the experimental data and the red line is a fit of Eq. (1) with $E_a = 2.982$ meV, $T_{VF} = 456$ K, and $f_0 = 1.8 \times 10^7$ Hz. The value of E_a is much smaller than that obtained for a PMN single crystal ($E_a = 78.6$ meV) [32], implying that it should be extremely easy for PNRs to merge into the surrounding structure [33]. The temperature at which the dielectric anomaly near 414 K has its maximum is independent of frequency and is attributed to the R-T transition.

C. Elastic and anelastic properties

In order to investigate the strain relaxational behavior and strain-related microstructural changes which occur in PIN-PZ-PMN-PT, RUS spectra were collected over a wide range of temperatures in the frequency range 100–1200 kHz. Figure 3(a) contains a stack of spectra from the $[001]_C$ PIN-PZ-PMN-PT crystal collected in a heating sequence from room temperature (295 K) to ∼700 K, with individual spectra offset up the y axis in proportion to the temperature at which they were collected. Figure 3(b) contains a similar stack collected from the $[001]_C$ PMN-28PT crystal. In each case, resonance peaks which have nearly fixed frequencies are from the alumina buffer rods. Peaks from the sample display strong temperature dependences, indicating that the ferroelectric transitions are accompanied by large variations in elastic constants. Stacks of primary spectra for both $[001]_C$ crystals collected during heating from ∼10 K to room temperature are shown in Fig. S3 (see Supplemental Material [20]). f^2 and Q^{-1} data obtained from fitting of individual peaks in these have been added to Figs. 3(c) and 3(d). It was not possible to follow the same resonance peak in both the high-temperature and low-temperature datasets so values of f^2 from the low-temperature resonances have been rescaled to match the high-temperature values at room temperature. The discontinuities in Q^{-1} at room temperature are experimental effects due to the fact that the sample rests directly on the transducers in the low-temperature instrument, while the acoustic signal is transmitted to and from

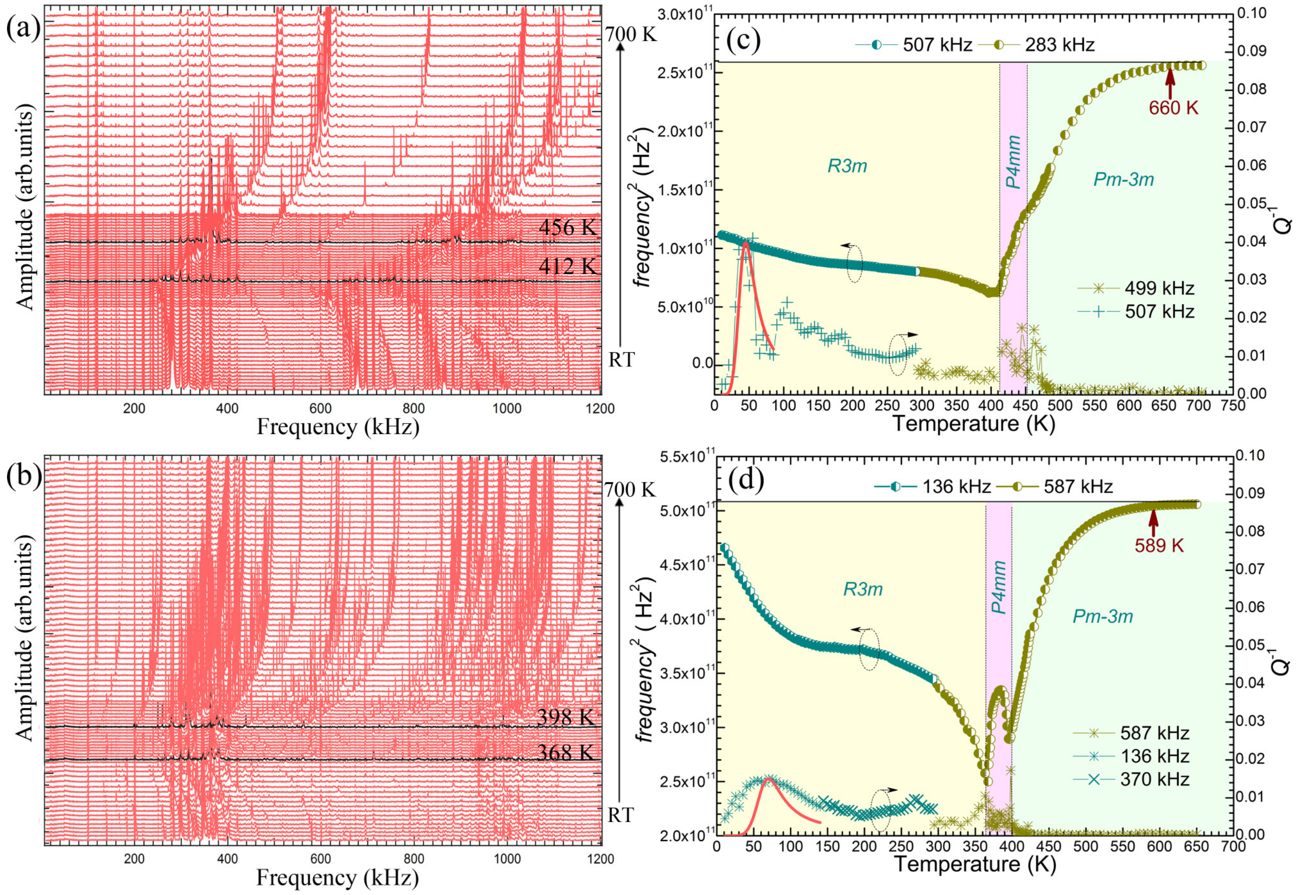

FIG. 3. (a) Stack of RUS spectra collected in a heating sequence, room temperature to ∼700 K, from the $[001]_C$ PIN-PZ-PMN-PT single crystal. Each spectrum has been offset up the y axis in proportion to the temperature at which it was collected. (b) Similar stack of spectra collected from the $[001]_C$ PMN-28PT single crystal. (c) $[001]_C$ PIN-PZ-PMN-PT single crystal. Temperature dependence of the squared frequency (f^2) and inverse mechanical quality factor (Q^{-1}) from fitting to a resonance peak with frequency near 283 kHz at high temperatures. These have been combined with data for a resonance peak near 507 kHz from spectra collected in a heating sequence from 10 to 295 K. f^2 values of the latter have been scaled to match up with the high-temperature data set at room temperature. (d) $[001]_C$ PMN-28PT single crystal. Data for f^2 and Q^{-1} obtained in a similar manner to that shown in (c).

the sample through alumina buffer rods in the high-temperature instrument.

The intrinsic acoustic resonances of a small object are dominated by shearing motions, and the square of their frequencies f^2 scales with the particular combination of elastic constant which controls each distortion. Given that a cubic crystal has only two shear elastic constants, it follows that the frequency variations observed in the stability field of the cubic structure represent the variations of C_{44} and $1/2(C_{11}-C_{12})$. Some of the resonant modes are dominated by C_{44} and some by $1/2(C_{11}-C_{12})$, but most depend on a mixture of the two [34]. Since all the resonances show similar changes in frequency with falling temperature, it is clear that there is marked softening of both elastic constants as the relaxor and ferroelectric transitions are approached from above. In the stability field of the rhombohedral structure, the resonance peaks are substantially broadened, signifying high acoustic loss which must relate to the mobility of microstructures coupled with strain in response to a dynamic stress. In detail, the f^2 data show two anomalies, corresponding to the R-T and T-C transitions, at 368 and 398 K for PMN-28PT but only one at ∼412 K for PIN-PZ-PMN-PT corresponding to the R-T transition. In PMN-28PT, the shear elastic constants have a sharp and discrete minimum at the T-C transition in a poled crystal, whereas the relaxor freezing process equivalent to this at ∼456 K in PIN-PZ-PMN-PT appears as only a small deviation in an interval of steep change. This demonstrates that any strains associated with the quasi-static PNRs can only be on a local length scale. Long-range strain fields only become established below the R-T transition where the main elastic anomaly is observed.

Changes in the elastic constants at a phase transition arise primarily from coupling of the driving order parameter with strain. In ferroelectric materials, the order parameter Q is usually viewed as the polarization caused by ionic shifts [10]. The symmetry breaking spontaneous strains are (e_1-e_2) and e_4, respectively, in the tetragonal and rhombohedral structure and coupling is of the form $\lambda(e_1-e_2)Q^2$ and $\lambda e_4 Q^2$. The expectation is that the pattern of softening will conform to the precepts of Landau theory for improper ferroelastic transitions such that a constant amount of softening will occur below the transition temperature for a second-order transition while a tricritical transition will lead to steep, nonlinear recovery. Formal coupling models have been developed for lead-based relaxor materials, such as PMN [35], PZN-PT [22], and PIN-PMN-PT [23], and these also apply in the present case. Softening by 10's of percent, as observed here, is typical of perovskites for which the magnitudes of the spontaneous strains are characteristically on the order of 0.1−1%. Complete working examples of these relationships are given elsewhere for $SrTiO_3$ [36] and $LaAlO_3$ [37].

Softening of the elastic constants ahead of an improper ferroelastic transition is due to fluctuations of the order parameter rather than to static strain/order parameter coupling. It is well understood that this is related to the development of local strain coupled to local polar precursor structures below the Burns temperature in ferroelectric and relaxor materials such as $BaTiO_3$ [38] and PMN [35,39,40]. On the basis of Figs. 3(c) and 3(d), the Burns temperatures for the PIN-PZ-PMN-PT and PMN-28PT crystals are ∼660 and ∼590 K, respectively. The lack of a significant elastic anomaly associated with the relaxor transition in PIN-PZ-PMN-PT, signifying the absence of any long-range macroscopic strain accompanying the freezing process of the PNRs, is closely analogous to the effect of local strain heterogeneity accompanying an octahedral tilting transition in $La_{0.6}Sr_{0.1}TiO_3$ [41]. When the degree of cation/vacancy disorder on the *A* sites is low, the tilting transition is accompanied by a significant symmetry-breaking strain. When the degree of disorder is high, the transition still occurs but there is no measurable macroscopic strain. In other words, the local strain heterogeneity caused by disordering suppresses the development of any long-range strain but does not suppress the transition itself. It follows that local strain heterogeneity associated with the introduction of In^{3+} and Zr^{4+} in PIN-PZ-PMN-PT can account for the suppression of any macroscopic strain associated with the local ferroelectric ordering, in comparison with PMN-28PT. This result coincides with the conclusion of He *et al.* [5] that a higher degree of relaxor character exists in PIN-PZ-PMN-PT due to the chemical substitution which also results in a shorter length scale for the PNRs. A further consequence of suppression of macroscopic strain will be to reduce the renormalization of the fourth-order coefficient of the Landau expansion in Q, making the ferroelectric transition more second order. This appears to be reflected in the reduced curvature of the elastic softening below the transition temperatures in PIN-PZ-PMN-PT, in comparison with PMN-28PT, which is typical of the difference between second-order and tricritical transitions (standard patterns are illustrated in Ref. [42]).

The influence of local strain heterogeneity at low temperatures should also be reflected in acoustic loss properties related to the mobility of strain fields at the boundaries of PNRs as well as of discrete twin walls under dynamic stress. In this context, the variations of Q^{-1} with temperature are slightly different between PIN-PZ-PMN-PT and PMN-28PT [Figs. 3(c) and 3(d)]. Firstly, the initial increases in Q^{-1}, with respect to low values for the cubic structure, reach values of ∼0.01 in PIN-PZ-PMN-PT, instead of ∼0.005 for the equivalent temperature interval in PMN-28PT. Secondly, high values up to ∼0.02 persist to lower temperatures and perhaps end up with a peak of ∼0.03 at ∼50 K for PIN-PZ-PMN-PT (though the signal-to-noise ratio in the primary spectra becomes very noisy at these lowest temperatures). A convenient phenomenological description of changes in acoustic loss as a function of temperature at constant frequency associated with a thermally activated process is

$$Q^{-1}(T) = Q_{\mathrm{m}}^{-1}\left[\cosh\left\{\frac{E_{\mathrm{a}}}{kr_2(\beta)}\left(\frac{1}{T}-\frac{1}{T_{\mathrm{m}}}\right)\right\}\right]^{-1}, \quad (2)$$

where E_a is the activation energy, k is the Boltzmann constant, and Q_m^{-1} is the maximum value of the peak in loss at temperature T_m [12,23,43]. Attempts to find fits of this expression to the data are shown in Figs. 3(c) and 3(d). Figure 3(c) shows the fit to what might be a typical single Debye loss peak with a single relaxation time [$E_a/r_2(\beta) = 179k$, $r_2(\beta) = 1$, $E_a = 15.4$ meV)]. The "fit" in Fig. 3(d) is shown to indicate that the broader interval of loss does not conform to a single relaxation process. The overall pattern of a wide temperature interval of high loss is thus more typical of loss mechanisms with a wide spread of relaxation times, as seen for example in $PbZr_{0.53}Ti_{0.47}O_3-Pb(Fe_{0.5}Ta_{0.5})O_3$ [44], rather than of the single thermally activated process typical of twin-wall motion and freezing, as seen for example in $KMnF_3$ [45]. Schiemer *et al.* [44] and Zhang *et al.* [6] have attributed this spread to the presence of unit-cell scale-strain heterogeneity and, in the present study, the effect is larger for PIN-PZ-PMN-PT than for PMN-28PT.

D. Comparison of dielectric and elastic properties

The dielectric constant represents susceptibility with respect to an applied electric field while elastic compliance represents susceptibility with respect to an applied stress field. These can have similar temperature dependences if the coupling between polarization and macroscopic strain is strong. On the other hand, the examples of PMN [35] and $0.5Ba(Zr_{0.2}Ti_{0.8})O_3-0.5(Ba_{0.7}Ca_{0.3})TiO_3$ [6] have shown that differences can be revealing of the nature of the relationship between strain and polarization on a local scale. Elastic compliance ($1/f^2$) and permittivity have therefore been plotted on the same graphs for PIN-PZ-PMN-PT and PMN-28PT in Figs. 4(a) and 4(b), respectively. The permittivity data for both materials show a similar pattern of two peaks, corresponding to the R-T and T/relaxor-C transitions, although there is an additional sharp peak at ∼390 K for PMN-28PT due to depoling during heating of the initially poled crystal. The elastic compliance results are quite different, however. Two peaks for PMN-28PT are at slightly different temperatures from the peaks in permittivity but clearly correspond to the R-T and T-C transitions, and the single peak for PIN-PZ-PMN-PT clearly corresponds to the R-T transition. The relaxor freezing behavior shows very obviously as a peak in permittivity and barely even a change in slope for compliance. This confirms the understanding of the PNR freezing process as giving rise to local ferroelectric dipoles without the development of any macroscopic symmetry-breaking shear strain. There is one peak in Q^{-1} and tan δ for PIN-PZ-PMN-PT [Fig. 4(c)] related to R-T, and two peaks for PMN-28PT [Fig. 4(d)] related to R-T and depolarization. High dieletric and acoustic loss between the relaxor freezing temperature and the R-T transition point shows that the there is some mobility of local ferroelectric domain walls on timescales of $\sim10^{-2}$–10^{-5} s, most likely dominated by 180° walls, and of local ferroelastic (90°) walls on a timescale of $\sim10^{-5}$–10^{-6} s.

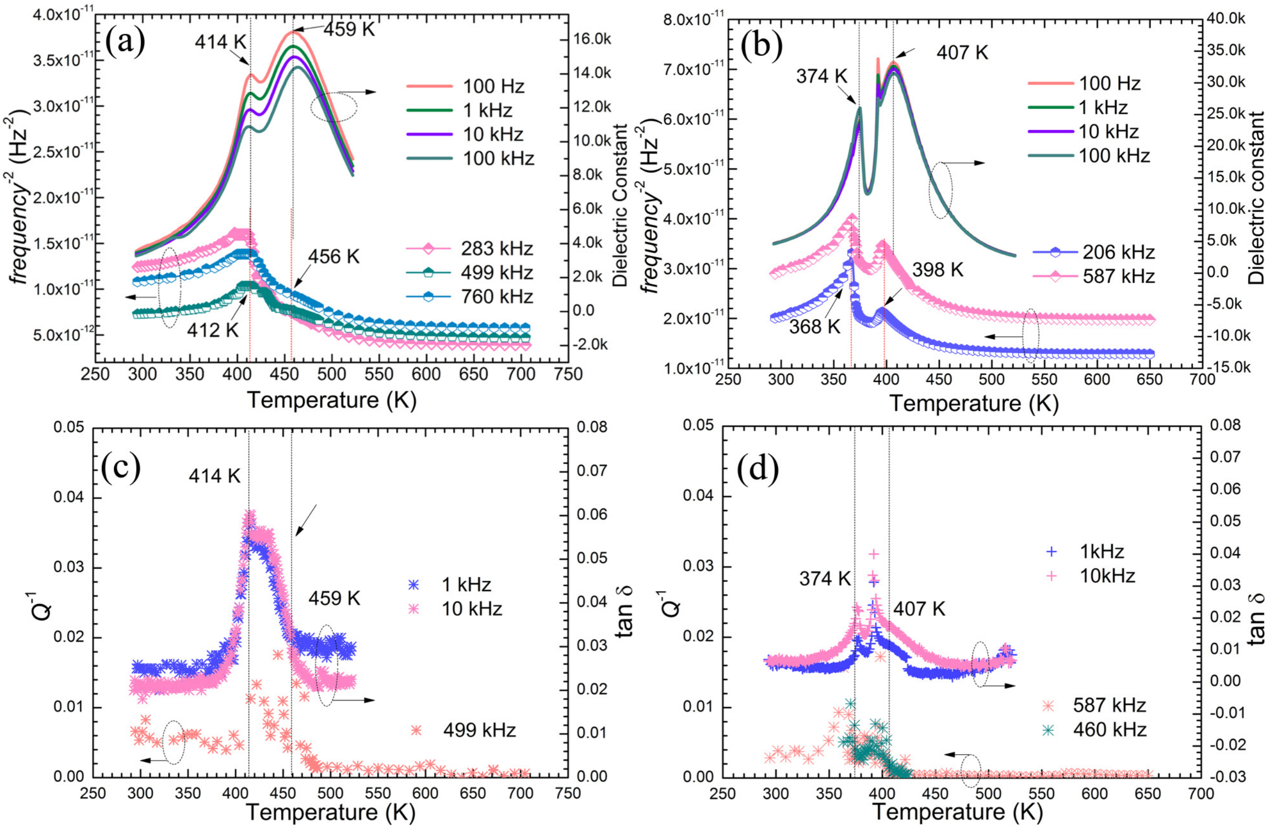

FIG. 4. Comparison of permittivity $1/f^2$ to represent elastic compliance, tanδ to represent dielectric loss and Q^{-1} to represent acoustic loss for (a) $[001]_C$ PIN-PZ-PMN-PT single crystal and (b) $[001]_C$ PMN-28PT single crystal. The RUS and dielectric data were collected in heating sequences from poled crystals.

E. PFM domain structures

Figure 5(a) shows that the microstructure of the $[001]_C$ crystal of PIN-PZ-PMN-PT, without applying dc voltage, at 303 K consisted of a typical labyrinthine domain pattern. PFM phase images obtained *in situ* at elevated temperatures show continuous variations of domain structures on the (001) surface in the temperature interval 303–503 K. On heating to 323 K [Fig. 5(b)] and 373 K [Fig. 5(c)] the basic pattern of domains remained essentially the same, although with weaker contrast and with additional variations within individual domains. At 423 K the domains had completely disappeared [Fig. 5(d)] and the change between 373 and 423 K illustrates the variation of local microstructure which may be associated with the macroscopic phase transition (R-T) observed by RUS and dielectric spectroscopy. At 453 K, 3 K below the Vogel-Fulcher freezing temperature, a domain structure could still be observed [Fig. 5(e)], but the phase angle indicated that it was not a typical ferroelectric-like piezoelectric domain structure. This dimly visible microdomain structure was still present at 503 K [Fig. 5(f)]. As shown in Fig. S4 (see Supplemental Material [20]), there is still a small residual ferroelectric response at 493 K. Temperature-dependent amplitude PFM images are given in Fig. S5 (see Supplemental Material [20]). Responses to the field applied by a PFM tip have been considered in much more detail by Kholkin *et al.* [14] in the case of PMN-10PT, and dynamic effects also influenced by symmetry breaking of the surface are likely to be responsible for some of the finer features seen in Fig. 5 and Supplemental Material [20].

In order to extract information about the average microstructural changes of the PIN-PZ-PMN-PT sample used here in a more quantitative manner, autocorrelation images $C(r_1,r_2)$ were obtained from the original PFM phase images using the autocorrelation transformation [16–18]:

$$C(r_1,r_2) = \sum_{x,y} D(x,y)D(x+r_1,y+r_2), \qquad (3)$$

where $D(x,y)$ is the value of the piezoresponse signal and $C(r_1,r_2)$ is the equivalent of a two-dimensional polarization-polarization correlation function. The symmetry and regularity of the polarization distribution is indicated by the shape of the resulting autocorrelation functions shown in Fig. 6(a). In this case, the short-range correlation length $\langle\xi\rangle$ could be obtained by fitting the curves of Fig. 6(a) at a small value of r (where r is the distance from the central maximum) using $C(r) = \sigma^2 \exp[-(\frac{r}{\langle\xi\rangle})^{2h}]$. The best fits at different temperatures are shown in Figs. 6(b1)–6(b6). The temperature dependence of $\langle\xi\rangle$ was also extracted from PFM images and the results are shown in Fig. 7. Values of $\langle\xi\rangle$ obtained for the (001) face are much smaller than the value of ~200 nm reported elsewhere for PMN-20PT [16], indicating that the strong RFs inhibit the aggregation of PNRs, which is entirely consistent with the more relaxor nature of the PIN-PZ-PMN-PT single crystal investigated here.

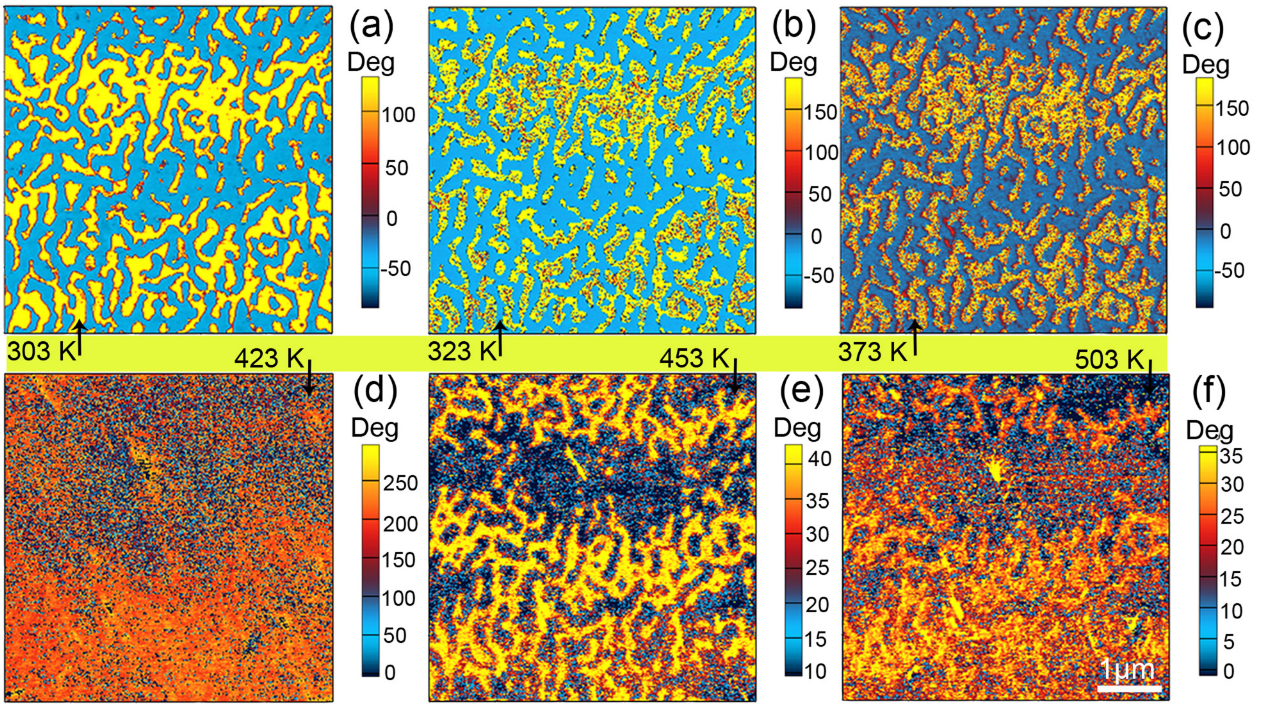

FIG. 5. Piezoresponse images of the (001) surface of the $[001]_C$ PIN-PZ-PMN-PT single crystal acquired *in situ* during a sequence of increasing temperature.

It is apparent from Fig. 7 that the average short-range order correlation radius falls with increasing temperature to 423 K. The driving force for such self-organization may be due to stress relief as the temperature increases, i.e., minimization of the free energy relating to the spontaneous strain, leading to the decreasing values of $\langle \xi \rangle$. Furthermore, the PNRs become smaller in volume and/or more disordered in polarity with heating [1,46], which may have a strong influence on $\langle \xi \rangle$. The development of PNRs is always accompanied by a change of volume strain. Therefore, when T_{VF} is approached, the slight increase of $\langle \xi \rangle$ could presumably be due to the variation of order parameter/strain coupling.

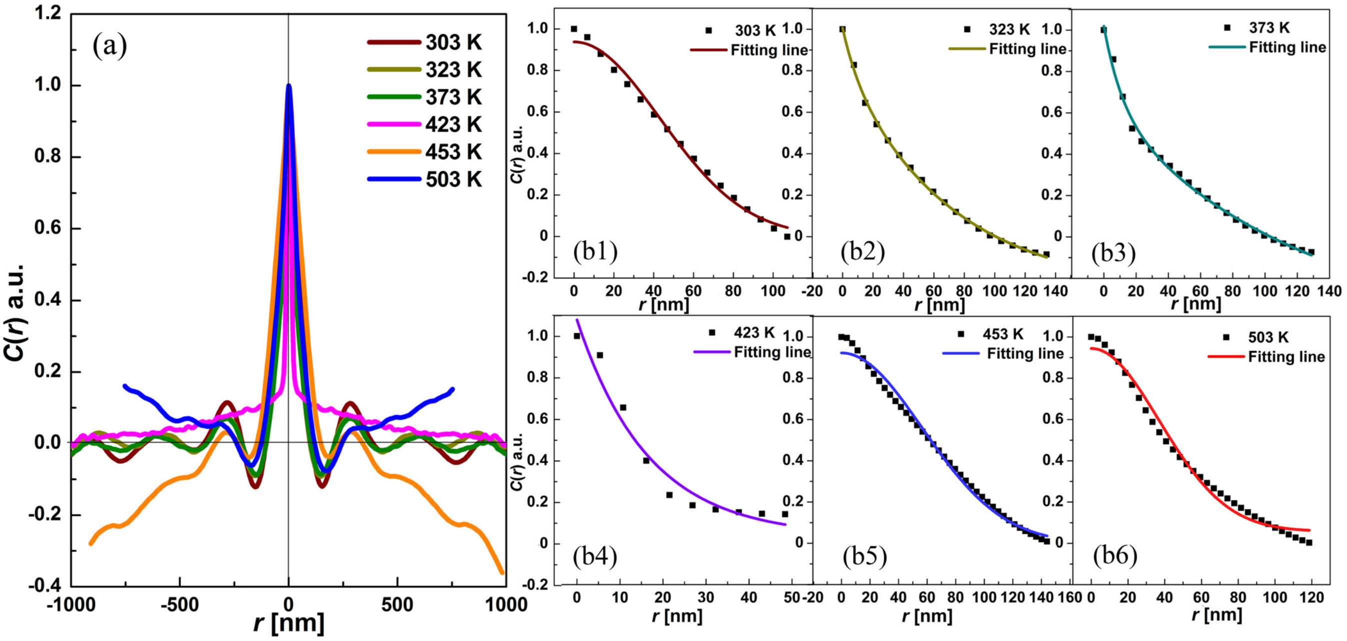

FIG. 6. (a) Cross section of the autocorrelation image along the direction of most pronounced oscillations of domains in PFM images from the (001) face of the $[001]_C$ crystal of PIN-PZ-PMN-PT, as shown in Fig. 5. (b1) 303 K, (b2) 323 K, (b3) 373 K, (b4) 423 K, (b5) 453 K, and (b6) 503 K show the averaged autocorrelation function at different temperatures and fits of the equation $C(r) = \sigma^2 \exp[-(\frac{r}{\langle \xi \rangle})^{2h}]$ used to extract values of the short-range correlation length $\langle \xi \rangle$.

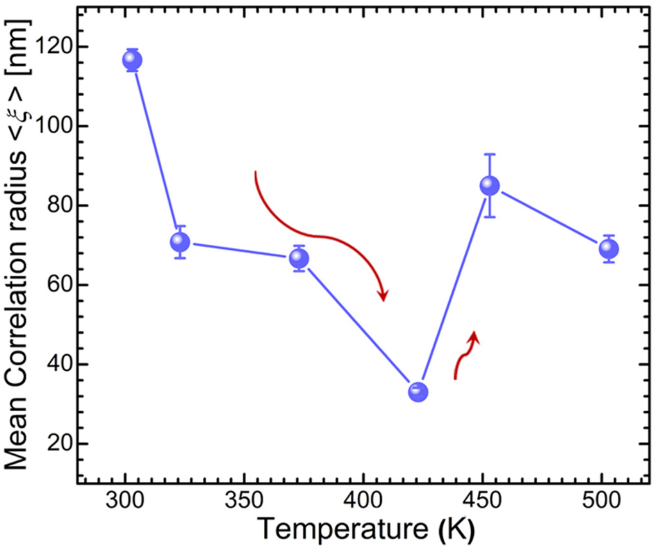

FIG. 7. Temperature dependence of the average correlation length $\langle \xi \rangle$ for microstructures observed by PFM on (001) surface of $[001]_C$ PIN-PZ-PMN-PT single crystal.

IV. CONCLUSIONS

Substitution of In^{3+} and Zr^{4+} in PMN-PT to give PIN-PZ-PMN-PT results in substantially improved temperature-insensitive properties, which may be attributed to the relaxor character associated with the development of random fields and a high R-T ferroelectric transition temperature. By comparing the elastic and anelastic properties of single-crystal PIN-PZ-PMN-PT and PMN-28PT, it has been shown that a significant effect of the chemical substitution of cations with different sizes is the development of local strain heterogeneity. This influence has been seen in the quite different form of elastic anomaly associated with Vogel-Fulcher freezing, as opposed to a discrete C-T transition, and high acoustic loss of the relaxor phase down to the R-T transition temperature. It is seen also in the change of the pattern of recovery of the shear elastic constants in the stability field of the rhombohedral structure from that expected for a tricritical transition to that expected for a second-order transition.

In effect, local strain heterogeneity acts to suppress the development of macroscopic shear strains without suppressing the development of local ferroelectric moments and must contribute substantially to the random fields which are widely considered to be at the heart of relaxor characteristics. The local strain effects have been seen also to influence the domain structure of the ferroelectric/improper ferroelastic rhombohedral structure and its response to a dynamical stress. Our understanding of these materials and selection for further engineering of their properties will be greatly enhanced by measurements of elastic/anelastic properties even if these are not the properties of primary technological interest.

ACKNOWLEDGMENTS

This work was supported by the National Basic Research Program of China (Grant No. 2013CB632900) and the National Natural Science Foundation of China (Grant No. 91333109). RUS facilities in Cambridge were established through grants from the Natural Environment Research Council and the Engineering and Physical Sciences Research Council of Great Britain to M.A.C.: Grants No. NE/B505738/1, No. NE/F17081/1, and No. EP/I036079/1. One of the authors (W.H.) thanks Professor Di Wu and Dr. Chen Li from Nanjing University for help with measuring the temperature-dependent PFM images.

---

[1] G. Y. Xu, J. S. Wen, C. Stock, and P. M. Gehring, Nat. Mater. **7**, 562 (2008).

[2] F. Li, S. J. Zhang, T. N. Yang, Z. Xu, N. Zhang, G. Liu, J. J. Wang, J. L. Wang, Z. X. Cheng, Z. G. Ye, J. Luo, T. R. Shrout, and L.-Q. Chen, Nat. Commun. **7**, 13807 (2016).

[3] F. Li, S. J. Zhang, Z. Xu, and L.-Q. Chen, Adv. Funct. Mater. **27**, 1700310 (2017).

[4] W. H. He, Q. Li, T. Jiang, F. P. Zhuo, and Q. F. Yan, Cryst. Eng. Commun. **18**, 5519 (2016).

[5] W. H. He, Q. Li, Y. Sun, X. Q. Xi, Y. L. Zhang, and Q. F. Yan, J. Mater. Chem. C **5**, 2459 (2017).

[6] L. Zhang, X. B. Ren, and M. A. Carpenter, Phys. Rev. B **95**, 054116 (2017).

[7] R. E. A. McKnight, T. Moxon, A. Buckley, P. A. Taylor, T. W. Darling, and M. A. Carpenter, J. Phys.: Condens. Matter. **20**, 075229 (2008).

[8] A. Migliori, J. L. Sarrao, W. M. Visscher, T. M. Bell, M. Lei, Z. Fisk, and R. G. Leisure, Physica B **183**, 1 (1993).

[9] R. G. Leisure and F. A. Willis, J. Phys.: Condens. Matter. **9**, 6001 (1997).

[10] M. A. Carpenter, J. F. J. Bryson, G. Catalan, and C. J. Howard, J. Phys.: Condens. Matter. **24**, 045901 (2012).

[11] E. K. H. Salje, M. A. Carpenter, G. F. Nataf, G. Picht, K. Webber, J. Weerasinghe, S. Lisenkov, and L. Bellaiche, Phys. Rev. B **87**, 014106 (2013).

[12] M. A. Carpenter, J. Phys.: Condens. Matter. **27**, 263201 (2015).

[13] R. K. Vasudevan, H. Khassaf, Y. Cao, S. J. Zhang, A. Tselev, B. Carmichael, M. B. Okatan, S. Jesse, L.-Q. Chen, S. P. Alpa, S. V. Kalinin, and N. Bassiri-Gharb, Adv. Funct. Mater. **26**, 478 (2016).

[14] A. Kholkin, A. Morozovska, D. Kiselev, I. Bdikin, B. Rodriguez, P. P. Wu, A. Bokov, Z.-G. Ye, B. Dkhil, L.-Q. Chen, M. Kosec, and S. V. Kalinin, Adv. Funct. Mater. **21**, 1977 (2011).

[15] Q. Li, Y. Liu, R. L. Withers, Y. H. Wan, Z. R. Li, and Z. Xu, J. Appl. Phys. **112**, 052006 (2012).

[16] V. V. Shvartsman, B. Dkhil, and A. L. Kholkin, Annu. Rev. Mater. Res. **43**, 423 (2013).

[17] V. V. Shvartsman, A. L. Kholkin, A. Orlova, D. Kiselev, A. A. Bogomolov, and A. Sternberg, Appl. Phys. Lett. **86**, 202907 (2005).

[18] V. V. Shvartsman and A. L. Kholkin, J. Appl. Phys. **101**, 064108 (2007).

[19] O. Noblanc, P. Gaucher, and G. Calvarin, J. Appl. Phys. **79**, 4291 (1996).

[20] See Supplemental Material at http://link.aps.org/supplemental/10.1103/PhysRevB.96.144109 for additional figures showing details of as-prepared $[001]_C$ PIN-PZ-PMN-PT single crystals, powder x-ray-diffraction patterns of PIN-PZ-PMN-PT and PMN-28PT collected at room temperature, low-temperature RUS spectra for (a) $[001]_C$ PIN-PZ-PMN-PT and (b) $[001]_C$ PMN-28PT relaxor single crystals, bipolar polarization hysteresis loop pattern of the $[001]_C$ PIN-PZ-PMN-PT single crystal at 493 K, and temperature-dependent amplitude images of $[001]_C$ PIN-PZ-PMN-PT single crystal obtained by PFM.

[21] A. Coelho, *Computer Code Coelho* (Coelho Software, Brisbane, Australia, 2007).

[22] Z. J. Xu, J. S. Wen, G. Y. Xu, C. Stock, J. S. Gardner, and P. M. Gehring, Phys. Rev. B **82**, 134124 (2010).

[23] G. F. Nataf, Q. Li, Y. Liu, R. L. Withers, S. L. Driver, and M. A. Carpenter, J. Appl. Phys. **113**, 124102 (2013).

[24] R. E. A. McKnight, M. A. Carpenter, T. W. Darling, A. Buckley, and P. A. Taylor, Am. Mineral. **92**, 1665 (2007).

[25] Q. Zou, H. Ruda, B. G. Yacobi, and M. Farrell, Thin Solid Films. **402**, 65 (2002).

[26] A. Kachouane, M. Addou, A. Bougrine, B. Elidrissi, R. Messoussi, M. Regragui, and J. C. Bernede, Mater. Chem. Phys. **70**, 285 (2001).

[27] E. Ramos-Moore, P. Ferrari, D. E. Diaz-Droguett, D. Lederman, and J. T. Evans, J. Appl. Phys. **111**, 014108 (2012).

[28] H. Liu, J. Chen, Y. Ren, L. X. Zhang, Z. Pan, L. L. Fan, and X. R. Xing, Adv. Electron. Mater. **1**, 1400051 (2015).

[29] S. J. Zhang and F. Li, J. Appl. Phys. **111**, 031301 (2012).

[30] A. K. Tagantsev, Phys. Rev. Lett. **72**, 1100 (1994).

[31] R. Pirc and R. Blinc, Phys. Rev. B **76**, 020101(R) (2007).

[32] D. Viehland, M. Wuttig, and L. E. Cross, Ferroelectrics **120**, 71 (1991).

[33] G. Y. Xu, D. Viehland, J. F. Li, P. M. Gehring, and G. Shirane, Phys. Rev. B **68**, 212410 (2003).

[34] L. J. Spalek, S. S. Saxena, C. Panagopoulos, T. Katsufuji, J. A. Schiemer, and M. A. Carpenter, Phys. Rev. B **90**, 054119 (2014).

[35] M. A. Carpenter, J. F. Bryson, G. Catalan, S. J. Zhang, and N. J. Donnelly, J. Phys.: Condens. Matter. **24**, 045902 (2012).

[36] M. A. Carpenter, Am. Mineral. **92**, 309 (2007).

[37] M. A. Carpenter, S. V. Sinogeikin, and J. D. Bass, J. Phys.: Condens. Matter. **22**, 035404 (2009).

[38] O. Aktas, M. A. Carpenter, and E. K. H. Salje, Appl. Phys. Lett. **103**, 142902 (2013).

[39] D. Viehland, S. J. Jang, L. E. Cross, and M. Wuttig, Philos. Mag. A **64**, 835 (1991).

[40] S. G. Lushnikov, A. I. Fedoseev, S. N. Gvasaliya, and Seiji Kojima, Phys. Rev. B **77**, 104122 (2008).

[41] C. J. Howard, Z. M. Zhang, M. A. Carpenter, and K. S. Knight, Phys. Rev. B **76**, 054108 (2007).

[42] M. A. Carpenter and E. K. H. Salje, Eur. J. Mineral. **10**, 693 (1998).

[43] M. Weller, G. Y. Li, J. X. Zhang, T. S. Ke, and J. Diehl, Acta Metall. **29**, 1047 (1981).

[44] J. A. Schiemer, I. Lascu, R. J. Harrison, A. Kumar, R. S. Katiyar, D. A. Sanchez, N. Ortega, C. Salazar Mejia, W. Schnelle, H. Shinohara, A. J. F. Heap, R. Nagaratnam, S. E. Dutton, J. F. Scott, B. Nair, N. D. Mathur, and M. A. Carpenter, J. Mater. Sci. **52**, 285 (2017).

[45] M. A. Carpenter, E. K. H. Salje, and C. J. Howard, Phys. Rev. B **85**, 224430 (2012).

[46] I.-K. Jeong, T. W. Darling, J. K. Lee, Th. Proffen, R. H. Heffner, J. S. Park, K. S. Hong, W. Dmowski, and T. Egami, Phys. Rev. Lett. **94**, 147602 (2005).